Low-Voltage IGZO Field-Effect Ultraviolet Photodiode

Shuang Song(宋双)[1,3], Huili Liang(梁会力)[1,2*], Wenxing Huo(霍文星)[4], Guang Zhang(张广)[5], Yonghui Zhang(张永晖)[6], Jiwei Wang(王绩伟)[3], and Zengxia Mei(梅增霞)[1,2*]

[1]*Songshan Lake Materials Laboratory, Dongguan 523808, China*
[2]*Institute of Physics, Chinese Academy of Sciences, Beijing 100190, China*
[3]*College of Physics, Liaoning University, Shenyang 110036, China*
[4]*Department of Instruments Science and Technology, School of Precision Instrument and Opto-electronics Engineering, Tianjin University, Tianjin 300072, China*
[5]*National Key Laboratory of Scattering and Radiation, Beijing 100039, China*
[6]*School of Physics and Optoelectronic Engineering, Shandong University of Technology, Zibo 255000, China*

(Received 2 April 2024; accepted manuscript online 27 May 2024)

In the era of Internet of Things (IoTs), an energy-efficient ultraviolet (UV) photodetector (PD) is highly desirable considering the massive usage scenarios such as environmental sterilization, fire alarm and corona discharge monitoring. So far, common self-powered UV PDs are mainly based on metal-semiconductor heterostructures or p–n heterojunctions, where the limited intrinsic built-in electric field restricts further enhancement of the photoresponsivity. In this work, an extremely low-voltage field-effect UV PD is proposed using a gate-drain shorted amorphous IGZO (a-IGZO) thin film transistor (TFT) architecture. A combined investigation of the experimental measurements and technology computer-aided design (TCAD) simulations suggests that the reverse current ($I_{\rm R}$) of field-effect diode (FED) is highly related with the threshold voltage ($V_{\rm th}$) of the parental TFT, implying an enhancement-mode TFT is preferable to fabricate the field-effect UV PD with low dark current. Driven by a low bias of -0.1 V, decent UV response has been realized including large UV/visible (R_{300}/R_{550}) rejection ratio (1.9×10^3), low dark current (1.15×10^{-12} A) as well as high photo-to-dark current ratio (PDCR, $\sim10^3$) and responsivity (1.89 A/W). This field-effect photodiode provides a new platform to construct UV PDs with well-balanced photoresponse performance at a low bias, which is attractive for designs of large-scale smart sensor networks with high energy efficiency.

DOI: 10.1088/0256-307X/41/6/068501

With the development of the Internet of Things (IoTs), various sensors are strongly desirable because they can collect massive and useful information to the IoT systems. Photodetector (PD) is one kind of the typical sensors since light is the most powerful source of information in the physical world.[1] As a part of the electromagnetic spectrum, ultraviolet (UV) light has wide applications in advanced communications, flame detection, air purification, and ozone sensing, etc.[2] The efficient detection of UV light will greatly enrich the function of IoT systems. Moreover, as the scale of IoTs increases and the number of sensors explodes, power supply is becoming an important issue for the distributed sensor system.[3,4] A little improvement on the energy efficiency of the single sensor will definitely decrease the whole power consumption. Thus, it is worthwhile to explore energy-efficient UV PDs with high performance.[5–8]

To avoid the bulky and expensive filters in traditional Si UV PDs, transparent amorphous oxide semiconductors (AOSs) are quite attractive as a smart UV sensor due to the suitable bandgap, large-area uniformity, high carrier mobility, and room-temperature fabrication feasibility.[9,10] Driven by a bias of several or tens of voltages, the reported AOS UV PDs usually demonstrate high responsivity.[9–14] However, owing to the asymmetry doping of oxide materials,[15] only metal/semiconductor Schottky diode or p–n heterojunction structure is feasible for self-powered UV PD at present.[5–7,16] The harsh demands for the interface quality and limited built-in electric potential make the responsivity of the self-powered UV PDs far below 1 A/W.[5–7,16,17] Therefore, it is necessary to develop new device architecture to balance the power consumption and device performance.

By shorting the gate and drain electrodes in thin film transistors (TFTs), a two-terminal field-effect diode (FED) is realized with typical rectifying behavior.[18,19] Based on this FED structure, Chang *et al.* reported a UV PD with NiO capping layer, where the reverse current ($I_{\rm R}$) of FED plays an important role on improvement of the photo-to dark current ratio (PDCR).[19] In this work, considering the mature device fabrication technology,[20,21] amorphous IGZO (a-IGZO) thin film was selected to fabricate the FED and explore its UV response at low bias. By using a combination of experimental design and numerical simulation, it has been revealed that the threshold voltage ($V_{\rm th}$) of TFT determines the $I_{\rm R}$ value of the correspond-

*Corresponding authors. Email: hlliang@iphy.ac.cn; zxmei@iphy.ac.cn
© 2024 Chinese Physical Society and IOP Publishing Ltd

ing FED. Driven by a reverse voltage (V_R) of −0.1 V, the photoresponsivity of FED is superior compared with self-powered devices. In addition, it is even comparable with normal UV PDs biased at several of voltages.

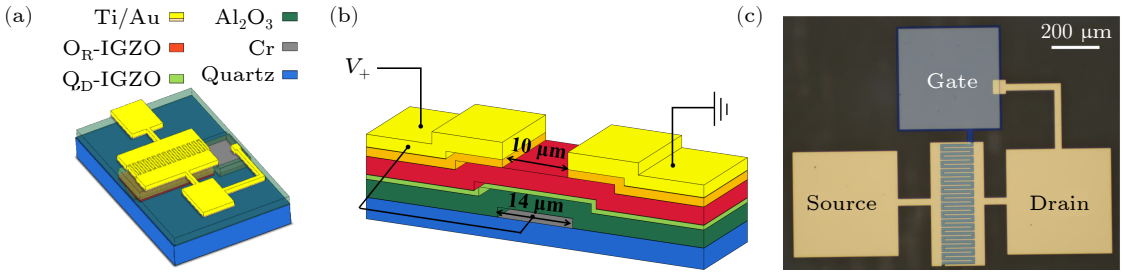

Fig. 1. Schematic diagram of the FED structure: (a) top view, (b) side view. (c) Optical microscope image of the completed device.

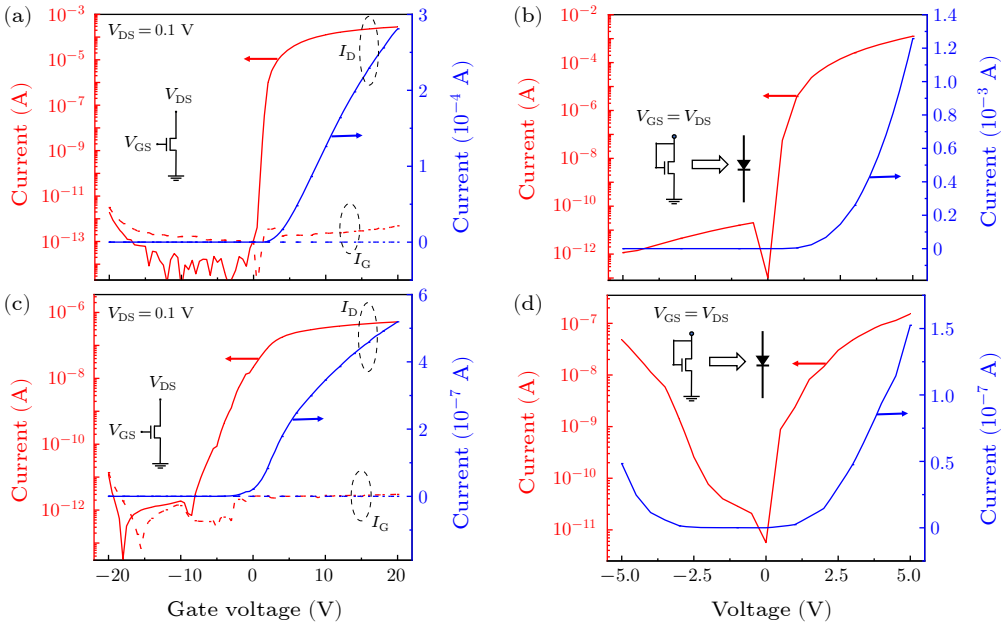

Fig. 2. (a) Transfer characteristics of S1-TFT. (b) I–V curve of S1-FED. (c) Transfer characteristics of S2-TFT. (d) I–V curve of S2-FED. Red lines are in logarithm scale and blue in linear scale.

Figure 1(a) depicts the schematic structure of the FED device. A Cr thin film was firstly deposited on quartz substrate by radio frequency (RF) magnetron sputtering, and after the UV lithography process, etched to form the winding bottom gate electrodes. A 100 nm Al_2O_3 dielectric layer was then synthesized by atomic layer deposition (ALD) at 200 °C. Considering the opposite dependence of field-effect mobility (μ_{FE}) and V_{th} on the carrier concentration of AOSs as reported previously, a dual-IGZO active layer was adopted in order to balance the TFT performance.[22,23] The dual a-IGZO channel, consisting of an oxygen-deficiency (O_D) and an oxygen-rich (O_R) IGZO layer, were prepared sequentially in the same RF sputtering chamber at 100 °C, with an atmosphere of pure Ar and 10 : 4 Ar/O_2 mixture, respectively. The O_D layer is for high carrier concentration and high μ_{FE} while the O_R layer is for the control of V_{th} of the TFT devices.[22] Two channel layers were designed. One is 8-nm O_D-IGZO/16-nm O_R-IGZO (S1), and the other is 8-nm O_D-IGZO/2-nm O_R-IGZO (S2). The transmittance spectra and surface morphology of IGZO thin films have been characterized as shown in Fig. S1 of the Supplementary Material. The dual-layer channels and Al_2O_3 insulating layer were patterned with a combination of UV lithography and wet etching by diluted hydrochloric acid (HCl) at room temperature and tetramethylammonium hydroxide (TMAH) solution at 60 °C, respectively. Source/drain electrodes were finally defined by UV lithography and lift-off process with the sequential deposition of Ti/Au thin films using RF sputtering technique. The width, length, and spacing of the fingers, as well as the overlap between the bottom gate and source/drain electrodes, are 145, 10, 10, and 2 μm, respectively.

Figure 1(b) displays the cross section of the device structure perpendicular to the fingers. Figure 1(c) is the top view of the completed device under the optical microscope, where it can be seen that the gate and drain electrodes are shorted via Ti/Au wire. It should be mentioned that TFT devices were fabricated with the same procedure except the shorted gate-drain electrodes in the last step. For simplicity, these devices are named as S1-TFT, S1-FED, S2-TFT, and S2-FED.

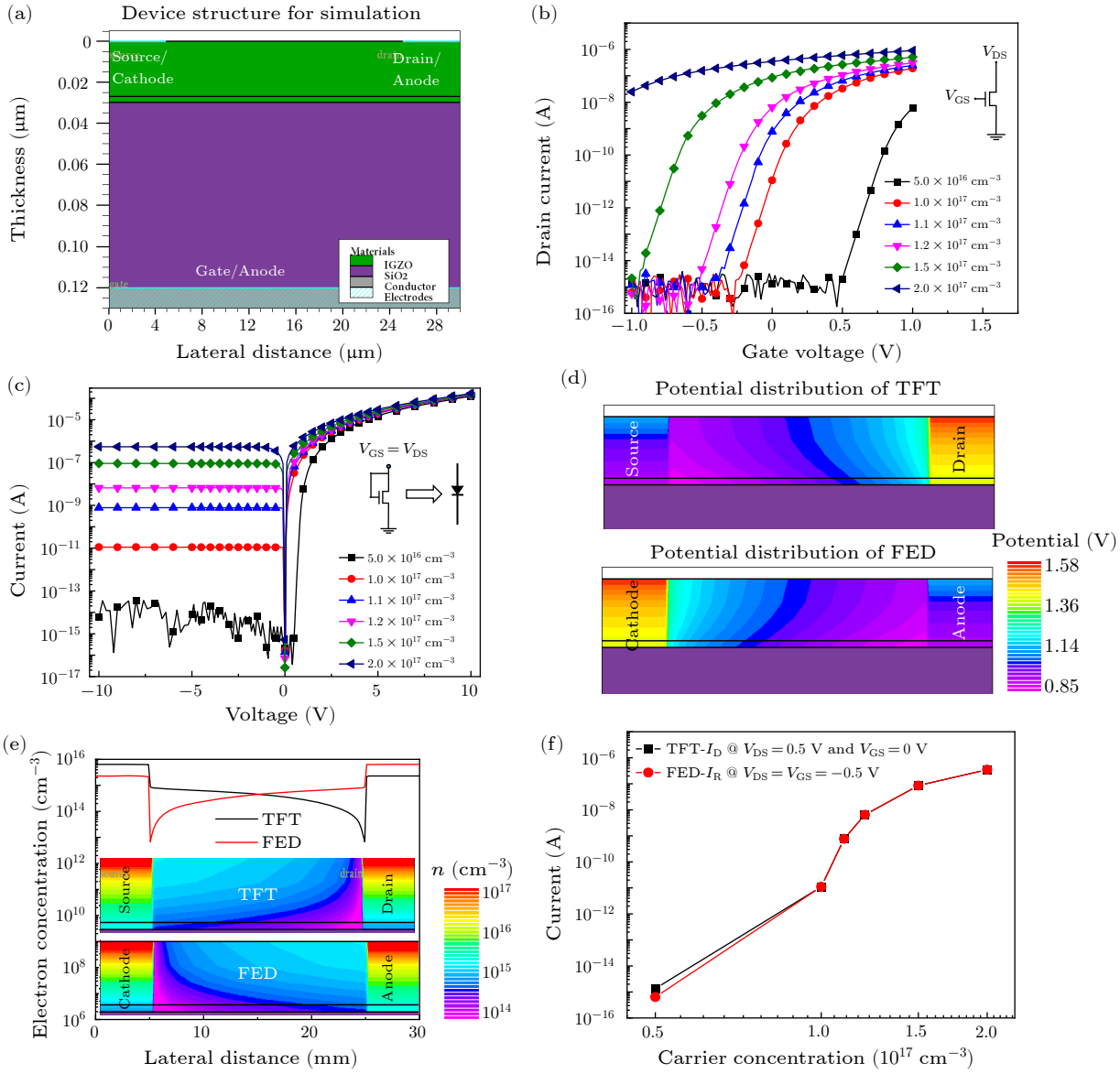

Fig. 3. (a) Schematic structure of the simulated device. Transfer curves of TFT (b) and I–V curves of corresponding FED (c) with different carrier concentrations in the IGZO active layer. Potential distribution (d) and electron concentration distribution (e) of the FED (biased at −0.5 V) and the parental TFT (biased at V_{GS} = 0 V and V_{DS} = 0.5 V). (f) Dependence of FED-I_R at −0.5 V and TFT-I_D at V_{DS} = 0.5 V and V_{GS} = 0 V on the carrier concentrations.

Figure 2 shows the electrical properties of the four devices. As reported previously, the carrier concentration of O_D a-IGZO is effectively enhanced via the introduction of oxygen vacancy (V_O) defects.[23] As a result, a large negative gate voltage is required to turn off the conductive channel. For S1-TFT, a typical transfer curve with near-zero V_{th} and sharp switching feature is observed [Fig. 2(a)], indicating that the 16 nm O_R-IGZO layer is effective to obtain an enhancement-mode TFT. The corresponding S1-FED demonstrates a high rectification ratio of 1.09×10^9 at ±5 V [Fig. 2(b)]. For S2-TFT, the top ultrathin O_R a-IGZO layer was grown for only 1 min with distributed granular morphology as demonstrated in our previous reports,[22,24] resulting in a negative V_{th}. In addition, O_D a-IGZO layer with abundant V_O defects brings additional trap states in the O_D-IGZO/O_R-IGZO homojunction and provides more sites to absorb oxygen molecules from the ambient air, leading to degraded μ_{FE} and SS values [Fig. 2(c)].[25] Meanwhile, the I_R of S2-FED increases more than 4 orders of magnitude compared with S1-FED [Fig. 2(d)]. Summary of device parameters for all samples can be referred to Table S1 in the Supplementary Material. Importantly, the I_R of S1-FED is in the level of $\sim10^{-12}$ A, rendering it possible as a low-voltage PD with high PDCR.

To find out the relationship between the device performance of FED and the corresponding TFT, technology computer aided design (TCAD) simulation was employed. The device structure is simplified as exhibited in Fig. 3(a), where 100 nm SiO_2 and 30 nm a-IGZO thin films are served as the oxide dielectric layer and the channel

layer, respectively. The carrier concentration of a-IGZO is set as 5.6×10^{16}, 1.0×10^{17}, 1.1×10^{17}, 1.2×10^{17}, 1.5×10^{17}, and $2.0 \times 10^{17}\,\mathrm{cm}^{-3}$. The electrical characteristics of FED is obtained by making the gate voltage (V_{GS}) equal to the drain voltage (V_{DS}). Figure 3(b) shows the transfer curves of the TFT with the above-mentioned carrier concentrations. The V_{th} shifts positively as the carrier concentration decreases, displaying a typical TFT behavior. However, the on-state current decreases a lot, showing an opposite dependence on the carrier concentration. That is the reason why a dual channel layer is constructed to modulate V_{th} in the experimental design. Figure 3(c) is the simulated I–V curves of the corresponding FED with conventional rectification performance. Importantly, the I_{R} value of the FED drops more than seven orders of magnitude as the carrier concentration decreases from $2.0 \times 10^{17}\,\mathrm{cm}^{-3}$ to $5.6 \times 10^{16}\,\mathrm{cm}^{-3}$. To reveal the underlying mechanism of I_{R} for FED, the electric potential and carrier concentration of the FED biased at $-0.5\,\mathrm{V}$ and the TFT biased at $V_{\mathrm{GS}} = 0\,\mathrm{V}$ and $V_{\mathrm{DS}} = 0.5\,\mathrm{V}$ have been extracted as shown in Figs. 3(d) and 3(e). A mirrored distribution can be clearly observed for both parameters. Further, the drain currents of TFT (TFT-I_{D}) at $V_{\mathrm{GS}} = 0\,\mathrm{V}$ and $V_{\mathrm{DS}} = 0.5\,\mathrm{V}$ and I_{R} of FED (FED-I_{R}) at $-0.5\,\mathrm{V}$ are taken from the curves in Figs. 3(b) and 3(c). Figure 3(f) illustrates the dependence of the above current values on the carrier concentrations, where a high convergence can be found. Therefore, the I_{R} of FED is highly related with the performance of the parental TFT. With a restricted gate bias condition of $V_{\mathrm{GS}} = V_{\mathrm{DS}}$, the shorted gate-drain electrode can be seen as the anode in FED.[18] When the anode is biased negatively at V_{R}, it can be regarded as a special operation mode of the TFT with $V_{\mathrm{GS}} = V_{\mathrm{DS}} = V_{\mathrm{R}} < 0$, which is equivalent to the bias condition of $V_{\mathrm{GS}} = 0\,\mathrm{V}$ and $V_{\mathrm{DS}} = \mathrm{abs}\,(V_{\mathrm{R}})$. Based on the above analysis, an enhancement-mode TFT is preferable to construct the field-effect UV PD with low dark current.

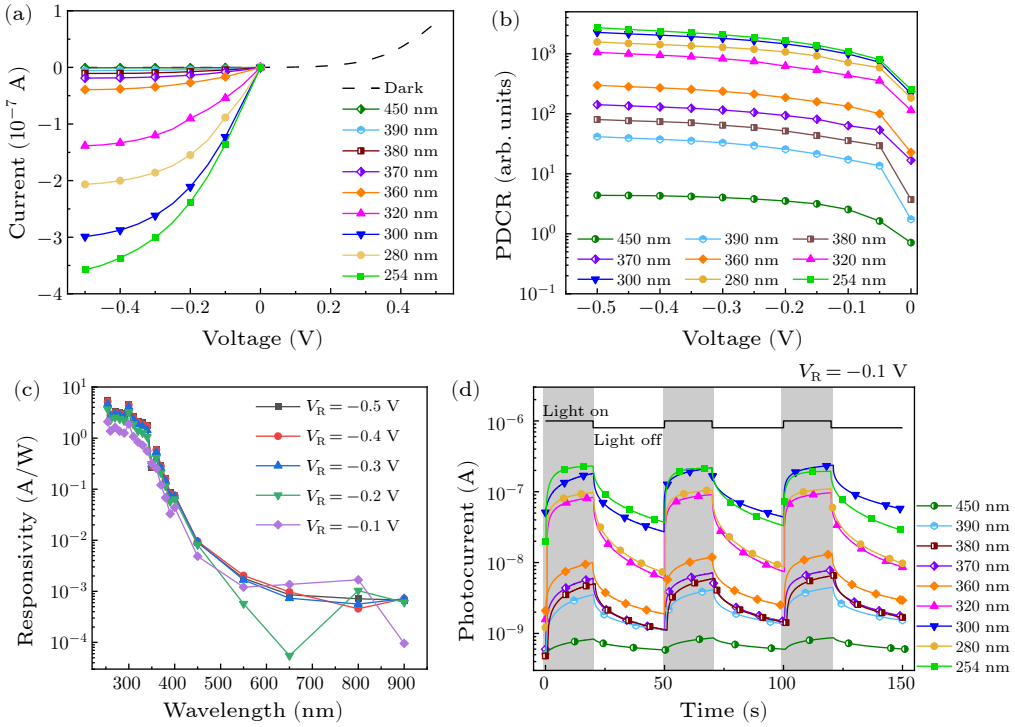

Fig. 4. (a) I–V curves in dark and under light illumination with different wavelengths. The light intensity was calibrated as $100\,\mu\mathrm{W/cm}^2$ by using a standard Si photodiode. (b) Dependence of PDCR values on V_{R} under different wavelengths. (c) Responsivity spectra at different reverse biases. (d) Transient response curves under periodical illumination with different wavelengths at a low bias of $-0.1\,\mathrm{V}$.

Further, the photoresponse behavior of S1-FED is investigated. Figure 4(a) shows the I–V curves in dark and under light illumination. Due to the presence of high-density sub-gap states above the valence band maximum (VBM) in AOS, weak photoresponse can be observed under the light illumination below bandgap.[23,26] Nevertheless, the I_{R} does not increase a lot until the wavelength of the incident light enters into the UV region. The light illumination makes the channel gradually on with the creation of photo-induced carriers.[27] Interestingly, these I–V curves manifest a trend like the traditional output curves for TFT devices. As the light wavelength becomes shorter, more photo-induced carriers are injected into the channel layer, similar to the effect of increasing positive V_{GS}.

Using the equation PDCR $= \frac{I_{\mathrm{ph}} - I_{\mathrm{dark}}}{I_{\mathrm{dark}}}$ (I_{ph} and I_{dark} are I_{R} values under light irradiation and in dark, respectively), the PDCR value is calculated. As shown in Fig. 4(b), PDCR grows slowly with the increase of V_{R}, demonstrating weak dependence on the reverse voltage.

The responsivity is defined as $R = \frac{I_{ph}-I_{dark}}{P\times S}$, where P is the power density of the incident light and S is the total illumination area of the device. A standard Si photodiode is used to calibrate the power density of the incident light. Figure 4(c) gives the photoresponsivity spectra under different reverse biases. At −0.1 V, the peak responsivity at 300 nm reaches 1.89 A/W and the UV/visible rejection ratio (R_{300}/R_{450}) is as high as 390, implying a decent UV detection performance. Moreover, the transient photoresponse measurements have been carried out under periodical illumination with different wavelengths [Fig. 4(d)]. All of these curves demonstrate good repeatability and stability with a common persistent photoconductivity (PPC) phenomenon, which is usually believed as the result of charge detrapping processes from ionized V_O defects in most oxide semiconductors.[27] The rising and decay time has been derived by using the principal of 20%–80% as shown in Fig. S2. It can be found that both the rising and decay times become longer and longer as the wavelength of the excitation light increases, consistent with the fact that the photoresponse from the longer wavelength below bandgap is mainly originated from the defects near VBM.[23] By applying a pulsed positive bias, it can be tentatively erased as shown in Fig. S3.

To concretely reveal the achievements of our a-IGZO field-effect PD, some critical parameters are summarized and compared with previous results (Table 1). With such a low reverse bias of −0.1 V, the peak responsivity of our FED is much higher than the self-powered devices,[5–7,16,17,28,29] and even comparable with those driven by the bias as large as 5 V,[28,30] indicating its great potential as a decent UV detector with low power consumption.

Table 1. Comparison of the main parameters for the reported self-powered UV PDs.

Material/structure	Rectification ratio	Wavelength (nm)	PDCR	Responsivity (A/W)	References
Au/a-IGZO/Au MSM	–	350	–	5×10^{-3} @0 V	[5]
Au/a-IGZO/Au MSM	–	350	$\sim10^2$ @±20 V	0.1×10^{-3} @0 V	[17]
a-IGZO/Si NWs p–n	–	380	–	0.53 @0 V	[6]
NiO/a-IGZO p–n	7.4×10^4 @±4 V	365	$\sim10^2$ @−4 V	0.029 @0 V	[7]
a-IGZO/p-Si p–n	330 @±1 V	325	181 @−3 V	8.0×10^{-3} @0 V 6.72 @−5 V	[28]
GaN/IGZO p–n	$>10^5$ @±5 V	340	$>10^5$ @0 V	0.26 @0 V	[16]
Ti/β-Ga_2O_3/Ni Schottky	∼20 @±10 V	254	$>10^5$ @−10 V	0.73×10^{-3} @0 V	[29]
ITO/IGZO/ITO MSM	–	405	2.9 @5 V	6 @5 V	[30]
DAL a-IGZO FED	1.09×10^9 @±5V	300	991 @−0.1 V	1.89 @−0.1 V	This work

In summary, we have constructed a low-voltage field-effect photodiode based on a gate-drain shorted dual-layer a-IGZO TFT. The combined TCAD simulation and experimental analysis manifest that an enhancement-mode TFT is desirable for the construction of field-effect photodiode with low I_R and large PDCR. Driven by a low V_R of −0.1 V, the FED device exhibits well-balanced UV detection performance compared with traditional self-powered PDs using both metal-semiconductor and p–n heterojunctions. This field-effect photodiode provides a new platform to construct high-performance UV PDs, which can be considered as a common device structure. Any photosensing material that can be applied as a channel layer for an enhancement-mode TFT can be designed as an energy-efficient field-effect photodiode just by shorting the gate and drain electrodes.

See the supplementary material including transmittance spectra and surface morphology of IGZO thin films (Fig. S1), summary of device parameters for all the samples (Table S1), derived rising and decay time against the wavelength from the time-dependent photoresponse curve (Fig. S2), the current of S1-FED under periodic light illumination (350 nm, 100 μW/cm^2), where the persistent photocurrent is tentatively erased by a pulsed square wave signal (15 V/1 s) (Fig. S3).

Acknowledgments. This work was supported by the National Natural Science Foundation of China (Grant Nos. 62174113, 12174275, and 61874139), and the Guangdong Basic and Applied Basic Research Foundation (Grant Nos. 2019B1515120057, 2023A1515140094, and 2023A1515110730).

References

[1] Yoo H, Lee I S, Jung S, Rho S M, Kang B H, and Kim H J 2021 *Adv. Mater.* **33** 2006091
[2] Chen H Y, Liu K W, Hu L F, Al-Ghamdi A A, and Fang X S 2015 *Mater. Today* **18** 493
[3] Akmandor A O, Yin H X, and Jha N K 2018 *IEEE Trans. Multi-Scale Comput. Syst.* **4** 914
[4] Nwadiugwu W P and Kim D S 2018 *3rd International Conference On Internet of Things: Smart Innovation and Usages (IoT-SIU)* (Bhimtal, India, 23–24 Febrary 2018) p 127
[5] Huang C Y, Peng T Y, and Hsieh W T 2020 *ACS Appl. Electron. Mater.* **2** 2976
[6] Huang C Y, Huang C P, Chen H, Pai S W, Wang P J, He X R, and Chen J C 2020 *Vacuum* **180** 109619
[7] Wang M Y, Zhang J W, Xin Q, Yi L, Guo Z K, Wang Y M, and Song A M 2022 *Opt. Express* **30** 27453
[8] Wang T, Liang H L, Han Z Y, Sui Y X, and Mei Z X 2021 *Adv. Mater. Technol.* **6** 2000945
[9] Cui S J, Mei Z X, Zhang Y H, Liang H L, and Du X L 2017 *Adv. Opt. Mater.* **5** 1700454
[10] Lai Y H, Wang I T, and Hou T H 2022 *Adv. Funct. Mater.* **32** 2200282

[11] Zhu R, Liang H L, Bai H, Zhu T, and Mei Z X 2022 *Appl. Mater. Today* **29** 101556

[12] Han Z Y, Song S, Liang H L, Shao H, Hu S G, Wang Y, Wang J W, and Mei Z X 2022 *Appl. Phys. Lett.* **120** 262102

[13] Pei Z, Lai H C, Wang J Y, Chiang W H, and Chen C H 2015 *IEEE Electron Dev. Lett.* **36** 44

[14] Han Z Y, Liang H L, Huo W X, Zhu X S, Du X L, and Mei Z X 2020 *Adv. Opt. Mater.* **8** 1901833

[15] Özgür Ü, Alivov Y I, Liu C, Teke A, Reshchikov M A, Doğan S, Avrutin V, Cho S J, and Morkoç H 2005 *J. Appl. Phys.* **98** 041301

[16] Liao Y K, Kim Y J, and Kim M 2023 *Chem. Eng. J.* **476** 146838

[17] Zhou H T, Li L, Chen H Y, Guo Z, Jiao S J, and Sun W J 2015 *RSC Adv.* **5** 87993

[18] Zhang Y H, Mei Z X, Cui S J, Liang H L, Liu Y P, and Du X L 2016 *Adv. Electron Mater.* **2** 1500486

[19] Chang C Y, Ko R M, Huang S J, Su M Y, Wu C H, and Wang S J 2022 *IEEE Electron Dev. Lett.* **43** 1299

[20] Wager J F 2020 *Inf. Display* **36** 9

[21] Hara Y, Kikuchi T, Kitagawa H, Morinaga J, Ohgami H, Imai H, Daitoh T, and Matsuo T 2018 *J. Soc. Inf. Display* **26** 169

[22] Huo W X, Mei Z X, Lu Y C, Han Z Y, Zhu R, Wang T, Sui Y X, Liang H L, and Du X L 2019 *Chin. Phys. B* **28** 087302

[23] Ide K, Nomura K, Hosono H, and Kamiya T 2019 *Phys. Status Solidi A* **216** 1800372

[24] Sui Y X, Liang H L, Chen Q S, Huo W X, Du X L, and Mei Z X 2020 *ACS Appl. Mater. Interfaces* **12** 8929

[25] Jeong J K, Won Yang H, Jeong J H, Mo Y G, and Kim H D 2008 *Appl. Phys. Lett.* **93** 123508

[26] Liang H L, Cui S J, Su R, Guan P F, He Y H, Yang L H, Chen L M, Zhang Y H, Mei Z X, and Du X L 2019 *ACS Photon.* **6** 351

[27] Jeon S, Ahn S E, Song I, Kim C J, Chung U I, Lee E, Yoo I, Nathan A, Lee S, Ghaffarzadeh K, Robertson J, and Kim K 2012 *Nat. Mater.* **11** 301

[28] Huang C Y, Li W Y, Hsiao Y H, Gao W N, and Chen C J 2020 *Smart Mater. Struct.* **29** 115019

[29] Liu Z, Wang X, Liu Y Y, Guo D Y, Li S, Yan Z Y, Tan C K, Li W J, Li P G, and Tang W H 2019 *J. Mater. Chem. C* **7** 13920

[30] Jia B, Zhang C, Liu M, Li Z, Wang J, Zhong L, Han C Y, Qin M, and Huang X D 2023 *Nat. Commun.* **14** 5330